Novel Composite Plastics Containing Silver(I) Acylpyrazolonato Additives Display Potent Antimicrobial Activity by Contact

Marchetti, F; Palmucci, J; Pettinari, C; Pettinari, R.; Condello, F; Ferraro, S.; Marangoni, M; Crispini, A; Scuri, S; Grappasonni, I.; Cocchioni, M; Nabissi, M; Chierotti, M.R; Gobetto, R.. Novel Composite Plastics Containing Silver(I) Acylpyrazolonato Additives Display Potent Antimicrobial Activity by Contact. CHEMISTRY-A EUROPEAN JOURNAL. 21 (2) pp: 836-850. DOI: 10.1002/chem.201404812

Novel Composite Plastics Containing Silver(I) Acylpyrazolonato Additives Display Potent Antimicrobial Activity by Contact

Fabio Marchetti,*† Jessica Palmucci,† Claudio Pettinari,*‡ Riccardo Pettinari,‡ Stefano Ferraro,† Mirko Marangoni,ζ Alessandra Crispini,‖ Stefania Scuri,‡ Iolanda Grappasonni,‡ Mario Cocchioni,‡ Michele R. Chierotti,§ Roberto Gobetto*§

† School of Science & Technology, and ‡School of Pharmacy, University of Camerino, Via S. Agostino 1, 62032 Camerino (MC), Italy, ζ Analisi Control S.r.l. - Via San Claudio, 5 - 62014 Corridonia (MC) Italy, § Dipartimento di Chimica, University of Torino, Via P. Giuria 7, and Centro di Eccellenza NIS, 10125 Torino, Italy, and ‖ Centro di Eccellenza CEMIF.CAL-LASCAMM, CR-INSTM (Unità della Calabria, Dipartimento di Chimica e Tecnologie Chimiche), Università della Calabria, I-87030 Arcavacata di Rende (CS), Italy

Keywords: silver(I) acyl-pyrazolonates, ^{15}N SS NMR, X-ray structures, PE embedding, PE composite materials, antimicrobial activity.

ABSTRACT: New silver(I) acylpyrazolonato derivatives displaying a mononuclear, polynuclear, or ionic nature, as a function of the ancillary azole ligands used in the synthesis, have been fully characterized by thermal analysis, solution NMR spectroscopy, solid-state IR and NMR spectroscopies, and X-ray diffraction techniques. These derivatives have been embedded in polyethylene (PE) matrix, and the antimicrobial activity of the composite materials has been tested against three bacterial strains (*E. coli, P. aeruginosa, and S. aureus*): Most of the composites show antimicrobial action comparable to PE embedded with $AgNO_3$. Tests by contact and release tests for specific migration of silver from PE composites clearly indicate that, at least in the case of the PE, for composites containing polynuclear silver(I) additives, the antimicrobial action is exerted by contact, without release of silver ions. Moreover, PE composites can be re-used several times, displaying the same antimicrobial activity. Membrane permeabilization studies and induced reactive oxygen species (ROS) generation tests confirm the disorganization of bacterial cell membranes. The cytotoxic effect, evaluated in $CD34^+$ cells by MTT (3-(4,5-dimethylthiazole-2-yl)-2,5-diphenyltetrazoliumbromide) and CFU (colony forming units) assays, indicates that the PE composites do not induce cytotoxicity in human cells. Studies of ecotoxicity, based on the test of Daphnia magna, confirm tolerability of the PE composites by higher organisms and exclude the release of Ag^+ ions in sufficient amounts to affect water environment.

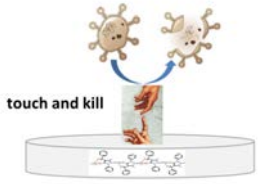

INTRODUCTION

In recent years the need for control of pathogenic microorganisms in contaminated environments has led to the development of antimicrobial materials[1] that can protect humans from infectious disease. Among the wide range of antimicrobial plastics, metal-polymer nanocomposites and, particularly, silver-polymers are the subject of increased interest.[2] Silver compounds are known to exhibit strong antimicrobial activity towards a broad spectrum of bacteria.[3] In low concentrations, silver is not toxic for human cells,[4] and it has been found to be effective in killing numerous types of infectious bacteria.[5]

Silver ions are proposed to react with electron donor groups (N, O, or S atoms), which are present in bacteria as, for example, amino, imidazole, and phosphate.[6] Although the exact antibacterial mechanism of colloidal silver nanoparticles remains unclear, it has been proposed that silver nanoparticles themselves are active.[7] However, more recent studies seem to indicate that, to be active, the silver nanoparticles (AgNPs) must first be converted to ionic silver, which is the effective antimicrobial species, through oxidation of the zero-valent silver, which limits the concentration of ionic silver available.[8]

Syntheses of AgNPs in commercially available polymers such as poly(vinyl alcohol) (PVA) or poly(vinylpyrrolidone) (PVP) have been carried out because of their excellent surface capping ability.[9] However, extensive release of the AgNPs from the materials could lead to environmental hazards,[10] and promote the development of resistant microbial strains.[11] More recent attempts to circumvent such limitations are based on microorganism-triggered release of AgNPs from biodegradable calcium phosphate carriers. In this approach, the growing bacteria dissolves the carrier containing nutrients and thereby releases the AgNPS, thus enabling a significant reduction of silver use.[12]

Our interest in silver derivatives and their potential application as antimicrobial agents recently led us to investigate different classes of ligands.[13, 14] We have previously shown that 4-acyl-5-pyrazolones[15] can be used to form silver(I) complexes that are mono-, di-, and even polynuclear.[16] Here, we have extended the previous studies to the synthesis of novel silver(I) complexes containing 4-acyl-5-pyrazolonate (Q) ligands with different electronic and steric features, and

several imidazoles L as ancillary ligands (Scheme 1), with the aim of obtaining

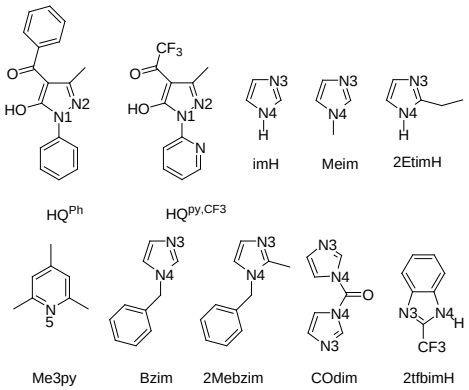

Scheme 1. Pro-ligands HQ and ligands L used.

a number of Ag^{I} derivatives with different nuclearity as potential antimicrobial agents to embed in plastics. Moreover, because polyethylene (PE) is one of the most common plastics, and is extensively used in packaging and containers for safe drinking water including bottles and taps, specific tests were carried out on PE disks with embedded Ag^{I} derivatives to assess the antimicrobial activity of composites against suspensions of *E. coli*, *P. aeruginosa*, and *S. aureus*, and to give insight on their mechanism of action. Our goal is to demonstrate that, in place of plastic composites of AgNPs with their associated side effects in terms of silver release and environmental impact, the embedding of insoluble silver(I) coordination polymers in a polymeric matrix may give rise to a new concept in the field of plastics with permanent antimicrobial activity: "contact action by polymer/polymer composites".

RESULTS AND DISCUSSION

Synthetic procedures

Derivative $Ag(Q^{Ph})$ (**1**) was obtained as a colorless precipitate by reaction between $AgNO_3$ and HQ^{Ph} in methanol using NaOMe as deprotonating agent (Scheme 2). Derivatives **2**-**5** were subsequently obtained by mixing an acetonitrile suspension of **1** with an excess or large excess of the corresponding imidazole, to afford Ag/Q^{Ph}/imidazole derivatives with 1:1:1 composition (derivatives **2** and **5**) or 1:1:2 (derivatives **3** and **4**), respectively (scheme 2). They are all air stable and quite high melting derivatives that are soluble and stable in dimethyl sulfoxide (DMSO) and acetonitrile and, in the case of **4** and **5**, also in alcohols and chlorinated solvents. Conductivity measurements carried out on solutions of **1**-**3** in DMSO and on solution of **4**-**5** in acetonitrile seem to indicate partial dissociation and formation of ionic species. This is in accordance, at least for **3**, with the ionic structure in the solid state (see X-ray data below), whereas in the case of **4** we can hypothesize a partial dissociation according to Equation (1):

$$[Ag(Q^{Ph})(Meim)_2] \leftrightarrows [Ag(Meim)_2]^+ + (Q^{Ph})^- \quad (1)$$

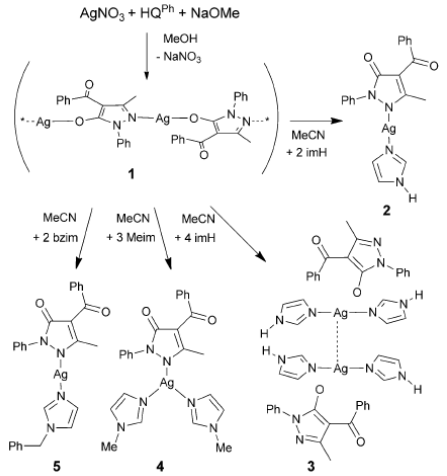

Scheme 2. Synthesis of derivatives **1**-**5**.

IR data of **1**-**5** show two strong absorptions in the range 1580-1653 cm^{-1} assigned to ν(C=O) stretching modes, likely indicating asymmetric chelation of Q^{Ph} through the carbonyl groups or even an ionic formulation of Q^{Ph} in the solid state,[15] as confirmed by X-ray data in the case of derivative **3**.

In ^1H NMR spectra of derivatives **2**-**5**, the integration ratio of H resonances of Q^{Ph} and imidazole ligand is in accordance with the anticipated 1:1 (derivatives **2** and **5**) or 2:1 formulation (derivatives **3** and **4**). Derivative **6** was obtained as a colorless precipitate by reaction of $AgNO_3$ with $HQ^{CF3,py}$ in methanol using NaOMe as deprotonating agent (Scheme 3). Derivatives **7**-**12** were subsequently obtained by mixing a solution of **6** in acetonitrile with equivalent amounts of the corresponding N-donor, to afford $Ag/Q^{py,CF3}$/N-donor derivatives with 1:1:1 composition, apart for di(imidazol-1-yl)methanone, which afforded derivative **10** with 2:2:1 composition (scheme 3). Derivatives **7**-**9** and **11**-**12** are monomeric substances (in the case of **9** it is further confirmed by X-ray data, see below), whereas **10** is likely composed by binuclear units, the ditopic di(imidazol-1-yl)methanone ligand bridging two $\{Ag(Q^{py,CF3})\}$ moieties. In the IR spectra of **7**-**12**, the ν(C=O) absorptions are found essentially unchanged with respect to those in free, neutral $HQ^{py,CF3}$, in accordance with the coordination of $Q^{py,CF3}$ primarily through the N atoms of the pyrazole and pyridine rings. TGA analyses show that **1**–**12** are thermally stable species, with decomposition not starting before 100°C for **4** and **7**–**9**, at approximately 150°C for **3** and **5**, at approximately 180°C for **12**, at approximately 200°C for **2** and well beyond for all the others. It is worth mentioning that derivative **10** decomposes in acetone/chloroform solution, according to the pathway described in the Scheme 3. The decomposition product 10' has been structurally analyzed (see below), proving the transformation of the COdim ligand into imidazole (imH), with the formation of a monomeric specie of general formula $[Ag(Q^{py,CF3})(imH)]$.

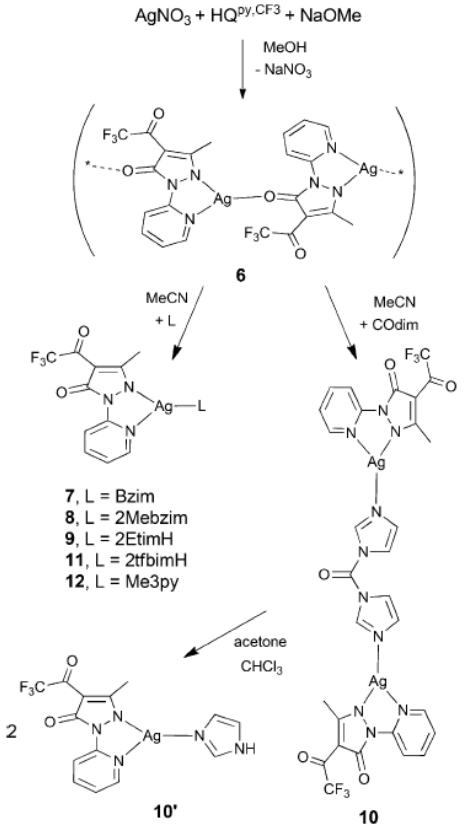

Scheme 3. Synthesis of derivatives **6**–**12**.

Solid State ^{15}N NMR Characterization

Solid-state NMR spectroscopy has provided more in-depth information on the coordination shift experienced by the N donor atoms interacting with the silver atom.[17] Earlier studies reported the NMR spectroscopic analysis of Ag^{I} complexes with substituted pyrazole ligands.[18] All 15N data are listed in Tables 1 and 2, and the ^{15}N CPMAS spectra are reported in Figures 1 (complexes **1**–**5**) and 2 (**6**–**12**). For nitrogen atom labeling, we refer to the Scheme 1. ^{15}N CPMAS spectra of the ligands and ^{13}C CPMAS spectra of all compounds with chemical shifts are reported in the Supporting Information (Figures S1, S2 and S3, respectively). In principle, the existence of two isotopes ^{107}Ag and ^{109}Ag (natural abundance 51.8 and 48.2 %, respectively) should give rise to two doublets with corresponding silver-nitrogen coupling constants. However, owing to very similar γ (magnetogyric ratio, $-1.089\cdot10^{7}$ and $-1.252\cdot10^{7}$ rad·T^{-1} s^{-1}, respectively) the relation between J couplings is J^{109}Ag-N/J^{107}Ag-N=1.15. Thus, the difference is often less than the spectral resolution. Indeed, for sp^3 nitrogen atoms, for instance N2 in all complexes, the coupling is expected to be smaller and the two resulting doublets appear as a broad signal. For cases in which the doublet can be resolved, an averaged value between J^{109}Ag-N and J^{107}Ag-N is reported. Concerning the HQ^{Ph} and $HQ^{py,CF3}$ ligands, the X-ray structure of HQ^{Ph} indicates the presence of two independent molecules in the unit cell[20] as confirmed by the splitting of the N2 resonance (253.5 and 251.9 ppm) in the ^{15}N CPMAS spectrum (Figure 1).

Table 1. ^{15}N chemical shifts (ppm) with assignment for the complexes **1**-**5** and the corresponding ligands HQ^{Ph}, imH, Meim, and Bzim. Peak multiplicity and J_{AgN} coupling constants (Hz) are reported in parentheses.

	N1	N2	N3	N4
HQ^{Ph}	165.6	253.5 251.9		
imH			220.5	149.4
Meim[19]			215	119
Bzim			234.3	153.7
1	167.1	207.6 (m, br)		
2	161.9	198.3 (m, br)	177.2 (m, br)	147.6
3	167.3	237.6	181.9 (m, br)	149.4 148.2
4	163.7	217.2 (br)	201.9 (d, 32) 198.6 (d, 46)	141.9 138.7
5	167.1	204.8 (m, br)	188.0 (m, br)	155.0 (br)

Table 2.^{15}N chemical shifts with assignment for the complexes **6**, **7**, **8**, **9**, **10**, **11** and **12** and the corresponding ligands $HQ^{py,CF3}$, Bzim, 2Mebzim, 2EtimH, COdim, 2tfbim, and Me3py. Peak multiplicity and J_{AgN} coupling constants (Hz) are reported between brackets.

	N1	N2	N(R2)	N3	N4	N5
$HQ^{py,CF3}$	163.3	239.7	137.2			
Bzim				234.3	153.7	
2Mebzim				234.9	143.8	
2EtimH				218.3	147.0	
COdim				220.6	149.1	
2tfbim				210.3	127.9	
Me3py[21]						260.7
6	168.7	236.3 232.0	208.6(br)			
7	168.3	229.7	182.6 (d, 86)	201.8 (m, br)	156.2	
8	165.4 br	218.6 br	183.1 (br)	200.8 (br)	147.7	
9	166.9	227.6	182.6 (d, 85)	201.1 (m, br)	140.7	
10	165.4 br	232.1	181.9 (m, br)	198.3 (br)	144.7	
11	166.6	215.2	174.2 (m, br)	200.9 (br)	125.1	
12	168.6	218.8	207.5			236.9 (d, 81)

On the other hand, the single set of signals in the ^{13}C CPMAS spectrum (see the Supporting Information) highlights the high similarity between the two molecules, both of which are characterized by the structure given in the Scheme 1. Concerning $HQ^{py,CF3}$, the ^{13}C and ^{15}N CPMAS spectra suggest the protonated structure reported in Scheme 4. This is characterized by a pyridinium cation, as confirmed by the 15N peak at 137.2 ppm (compared with the pyridyl signal, which resonates at ca. 280 ppm). For complexes **1**, **2**, **4**, and **5** (Figure 1, Table 1) the N2 chemical shift suggests nitrogen coordination to the silver atom according to Scheme 2. Indeed, all signals experience coordination shifts toward lower frequencies around 45.5 ppm. For sample **4**, the small value of the measured JAgN couplings with respect to those reported

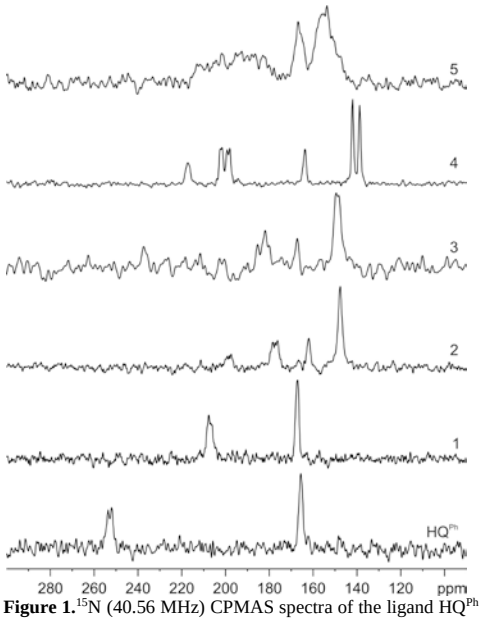

Figure 1. ^{15}N (40.56 MHz) CPMAS spectra of the ligand HQ^{Ph} and complexes **1**-**5** recorded with a spinning speed of 9 kHz.

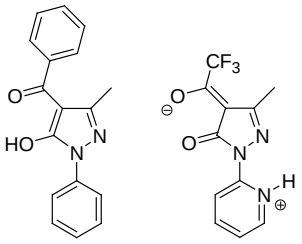

(a) HQ^{Ph} (b) $HQ^{py,CF3}$

Scheme 4. Structure of proli-gands HQ^{Ph} and $HQ^{py,CF3}$.

previously[22] suggests weaker Ag-N bonds (as confirmed by the X-ray structure, see below).

The ^{15}N CPMAS spectrum of **3** is consistent with the X-ray structure (see below): the absence for the N2 signal of either splitting or broadening due to JAgN coupling confirms the lack of coordination to the metal, whereas the small shift toward lower frequencies (ca. 16 ppm) with respect to the free ligand is consistent with the formation of a cocrystal between the free HQ^{Ph} ligand and the Ag(imH) dimer. Interestingly, in the series of compounds **6**–**12** (Figure 2, Table 2), the shift upon coordination of the N2 signal is smaller than in the previous series (ca. 13 ppm, max. 24.5 ppm). This can be related to the different coordination type of the silver atom, which leads to longer Ag-N distances (see X-ray structure below). The N_{Py} signal undergoes a high frequency shift with

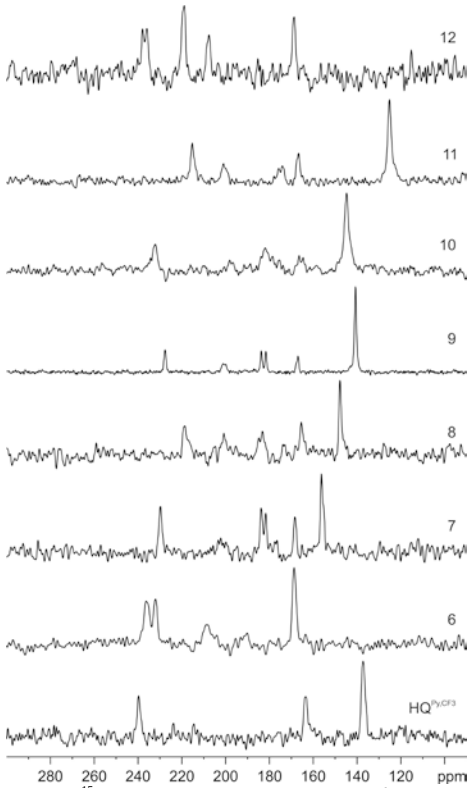

Figure 2. ^{15}N (40.56 MHz) CPMAS spectra of the ligand $HQ^{py,CF3}$ and complexes **6**-**12** recorded with a spinning speed of 9 kHz.

respect to the pyridinium position of the free ligand. However, it resonates at lower frequency compared with that of the pyridine, indicating that N_{Py} is coordinated to the metal. The splitting of some resonance in the ^{13}C and ^{15}N CPMAS spectra of **6** suggests the presence of two independent molecules in the unit cell. The number of peaks in the ^{13}C and ^{15}N NMR data of complex **10** suggests a highly symmetric environment of the complex: indeed, for instance, only one signal is observed for N4 (δ_{15N}= 144.7 ppm) and for the methyl (δ_{13C}=19.4 ppm). In 12, coordination of the Me3py ligand through the nitrogen atom is confirmed by the N5 shift from 260.7 (free ligand) to 236.9 ppm (complex).

Crystallography

The X-ray crystal structure analysis of derivative 3 confirmed the ionic nature of the isolated specie in the crystalline solid state (Figure 3 a). The silver cation is built up through coordination of the neutral nitrogen atoms of two imH ligands to the Ag^{I} ion, in a distorted linear geometry [N(3)-Ag-N(5) of 167.3(1)°]. The Q^{Ph} ligand is found as counter ion in its unprotonated form $(Q^{Ph})^{-}$ and therefore is not coordinated to

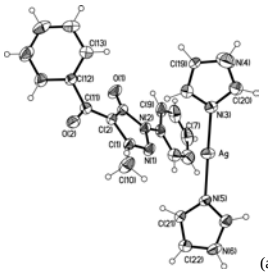

(a)

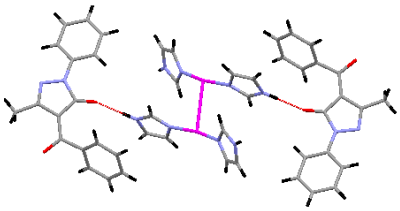

(b)

Figure 3. a) Perspective view of the asymmetric unit content of **[Ag(imH)$_2$][Q^{Ph}] (3)** with atomic numbering scheme (ellipsoids at the 40% level) and b) crystal packing views of **3** showing the formation of columns and relative intermolecular interactions.

the silver metal center. The C(3)-O(1) bond distance of 1.248(3) Å proves that the deprotonation arises from the original keto form of the Q^{Ph} molecule, as observed in similar HQ^{R} pyrazolones.[23] The [Ag(imH)$_2$][Q^{Ph}] unit, when repeated through an inversion center, gives rise to a binuclear structure in which the two silver cations are joined through a strong Ag-Ag interaction of 3.202(1) Å (Figure 3 b). The so-formed silver dimer strongly interacts with the anions through hydrogen bonds of the N-H···O type, between one imidazole coordinated ligand and the keto-oxygen atom of the [Q^{Ph}]$^-$ anion [N(6)-O(1)^i 2.691(3) Å, N(6)-H(6)···O(1)^i 173.5°, i=x, y, z+1]. In contrast to derivative **3**, the single-crystal X-ray analysis of complex **4** demonstrated the neutral nature of the latter, at least in the solid state, confirming the general formula [Ag(Q^{Ph})(Meim)$_2$]. The Q^{Ph} ligand coordinates the silver(I) ion in a monodentate fashion, through the negatively charged nitrogen atom (Figure 4a).

Two Meim ligands complete the Ag^I coordination sphere, bounding the metal ion though their nitrogen atom, and generating an overall pseudo trigonal-planar distorted geometry.

The maximum deviation from trigonality is due to the presence of the rotationally free phenyl ring of the Q^{Ph} ligand, causing an enlargement of the N(1)-Ag-N(5) angle to 128.7(1)°. The central pyrazole ring of the Q^{Ph} ligand is found to be nearly orthogonal with respect to the mean coordination plane, with a torsion angle of about 50°. As a consequence, a CH/π attractive intermolecular interaction between the N ortho-hydrogen atom of one coordinated Meim ligand and the

molecules in the unit cell.
The number of peaks in the ^{13}C and ^{15}N NMR data of complex **10** suggests a highly symmetric environment of the complex: indeed, for instance, only one signal is observed for N4 (δ_{15N} = 144.7) and for the methyl (δ_{13C} = 19.4). In sample **12**, the coordination of the Me3py ligand through the nitrogen atom is confirmed by the N5 shift from 260.7 (free ligand) to 236.9 (complex) ppm.

Crystal Structures Analysisof 3, 4, 9, 10′ and 12.
The X-ray crystal structure analysis of derivative **3** has confirmed the ionic nature of the isolated specie in the crystalline solid state (Figure 4a). The silver cation is built up through the coordination of the neutral nitrogen atoms of two imidazole imH ligands to the Ag(I) ion, in a distorted linear geometry (N(3)-Ag-N(5) of 167.3(1)°). The Q^{Ph} ligand is found as counterion in its unprotoned form $(Q^{Ph})^-$ and therefore not coordinated to the silver metal centre. The C(3)-O(1) bond distance of 1.248(3) Å proves that the deprotonation arises from the original keto-form of the Q^{Ph} molecule, as already observed in similar HQ^R pyrazolones.[31] The overall geometry of the $\mathbf{[Q^{Ph}]^-}$ anion is not planar, where the major deviation is related to the quasi orthogonality of the rotationally free phenyl ring with respect to the central pyrazole one [dihedral angle between the N(1)-N(2)-C(1)-C(2)-C(3) and C(12)/C(17) mean planes of 64.5(1)°].
The $\mathbf{[Ag(imH)_2][Q^{Ph}]}$ unit, when repeated through an inversion centre gives rise to a dimeric structure, in which the two silver cations are joint with a strong Ag---Ag interaction of 3.202(1) Å (Figure 4b). The so formed silver dimer strongly interacts with the anions through hydrogen bonds of the N-H---O type, between one imidazole coordinated ligand and the keto-oxygen atom of the $\mathbf{[Q^{Ph}]^-}$anion [N(6)—O(1)^i 2.691(3) Å, N(6)-H(6)—O(1)^i 173.5°, *i* = *x*, *y*, *z*+1].
Differently from derivative **3**, the single crystal X ray analysis of complex **4** has demonstrated its neutral nature at least in the solid state, confirming the general formula $\mathbf{[Ag(Q^{Ph})(Meim)_2]}$. The Q^{Ph} ligand coordinates the silver(I) ion in a monodentate fashion, through the negatively charged nitrogen atom (Figure 5a).

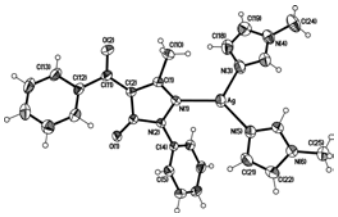

(a)

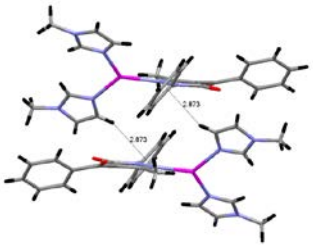

(b)

Figure 5. Perspective view of the asymmetric unit content of $\mathbf{[Ag(Q^{Ph})(Meim)_2]}$ **(4)** with atomic numbering scheme (ellipsoids at the 40% level) (a) and the formation of dimmers in the crystal packing with CH/π attractive intermolecular interactions (b).
Two imidazole Meim ligands complete the Ag(I) coordination sphere, bounding the metal ion though their nitrogen atom, and generating an overall pseudo trigonal-planar distorted geometry. The maximum deviation from trigonality is due to the presence of the rotationally free phenyl ring of the Q^{Ph} ligand , causing an enlargement of the N(1)-Ag-N(5) angle of 128.7(1)°. The central pyrrole ring of the Q^{Ph} ligand is found to be nearly orthogonal with respect to the mean coordination plane, with a torsion angle of about 50°.
As a consequence, a CH/π attractive intermolecular interaction between the N-ortho hydrogen atom of one coordinated Meim ligand and the rotationally free phenyl ring of Q^{Ph} is the structural feature characterizing complex **4** crystal packing (Figure 5b). Very short H---phenyl plane distances characterize this interaction, all geometrical parameters being indicative of its presence.[32]
Moving from the HQ^{ph} to the $HQ^{py,CF3}$ ligand, the ligand coordination mode with respect to the Ag(I) ion changes drastically. Indeed, the crystal structure determination of complex **9** proves the mono-anionic N_2-chelating mode of the $[Q^{py,CF3}]$ligand, with the Ag(I) coordination sphere completed by the imidazole **2EtimH** bound through its nitrogen atom (Figure 6a).

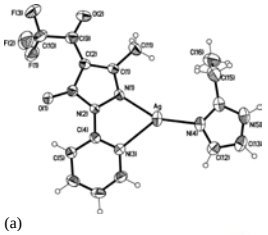

(a)

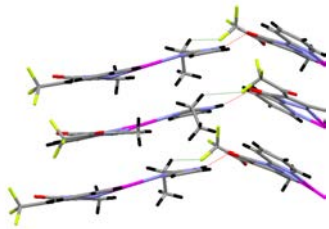

(b)

Figure 6. Perspective view of the asymmetric unit content of $\mathbf{[Ag(Q^{py,CF3})(2EtimH)]}$ **(9)** with atomic numbering scheme (ellipsoids at the 40% level) (a) and crystal packing views of **9** showing the formation of columns and relative intermolecular interactions (b).
The bond distances and angles around the Ag(I) ion are comparable to those found in the crystal structure of an analogous Ag(I) complex of $HQ^{py,CF3}$ ligand recently reported, containing the imidazole Meim similarly coordinated.[15a] However, in the case of complex **9**, a greater asymmetry between the Ag-N bond distances within the NN-chelated ring is found with respect to the already reported derivative, being the distance with the pyridine nitrogen atom longer than the other (Ag-N(1) and Ag-N(3) distances of 2.240(3) Å and 2.392(3) Å, respectively). The geometry around the central metal ion could be defined as very distorted trigonal-planar, being the N(1)-Ag-N(3) "bite" angle of 71.4(1)° and the angle N(1)-Ag-N(4) of 154.7(1)°. The overall planarity of the molecule is broken by both the high distortion from planarity of the NN-chelated ring (internal torsion angle around the N(2)-C(4) bond of 10.2(4)°) and the slight rotation of the **2EtimH** ligand with respect to the NN-chelated ring, being the dihedral angle between their mean planes of 8.5(1)°.The packing mode of complex **9** is dominated by the formation of columns of molecules stacked on the top of each other slightly shifted with a repetitive Ag---Ag intermolecular distance of 3.9 Å (Figure 6b). The interaction between columns is ensured by the presence of strong N-H—O

hydrogen bonds [N(5)---O(1)^{i} 2.853(4) Å, N(5)-H(5a)—O(1) 163.6°, *i* = x, -y+2, z-1/2] and intermolecular interactions involving the fluorine atoms of the CF_3 groups and one of the methylene hydrogen atoms [C(15)---F(2)^{i} 3.376(5) Å, C(15)-H(15a)—F(2) 135.0°]. As previously anticipated, both the decomposition product **10**$^{'}$ and complex **12** have been structurally analyzed, and their characterization has confirmed the same type of N_2-chelating mode of $Q^{py,CF3}$, seen in the case of complex **9** (Figure 7a,b). In both cases, the distorted trigonal-planar geometry around the silver ion is reached through its coordination to the imidazole ligand nitrogen atom (**imH** and **Me3py** in **10**$^{'}$ and **12**, respectively), with N-Ag-N "bite" angles within the NN-chelated ring of 70.5(1)° and 71.1(1)° in the two molecules of the asymmetric unit in **10'** and 70.9(1)° in **12**.

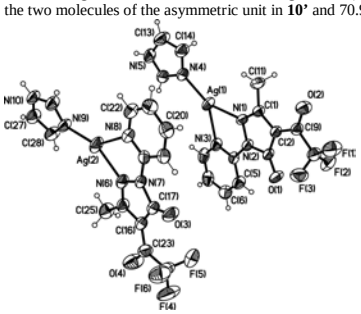

(a)

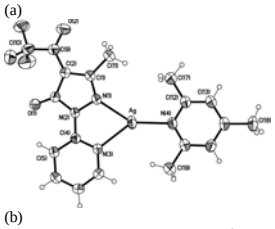

(b)

Figure 7. Perspective view of the asymmetric unit content of **[Ag($Q^{py,CF3}$)(imH)] (10**$^{'}$**)** (a)and **[Ag($Q^{py,CF3}$)(Me3py)] (12)** (b) with atomic numbering scheme (ellipsoids at the 40% level).

The same asymmetry between the two Ag-N bond distances with the coordinated $\mathbf{Q^{py,CF3}}$ligand seen in the case of derivative **9**, is found in both **10**$^{'}$ and **12** complexes, being less pronounced in the case of **12** (Table 3). While the NN-chelated ring of both molecules in the asymmetric unit of **10**$^{'}$ is found to be closer to planarity, as shown by the torsion angles around the N-C internal bond of 1.4(4)° and 0.65(4)°, respectively, derivative **12** shows a similar distortion seen in **9**, with a torsion angle of 7.2(4)°.

In both cases the rotationally free imidazole ligand is found slight rotated with respect to the NN-chelated ring, being the dihedral angles between their mean planes of 10.1(1)° and 12.6(1)° in **10'** and 5.9(1)° in **12**.

Table 3 Relevant bond lengths (Å) and angles (°) for complexes **9, 10**$^{'}$and **12.**

	9	**10**$^{'}$	**12**
		bond lengths	
Ag-N(1)	2.240(3)	2.230(2), 2.233(3)	2.306(2)
Ag-N(3)	2.392(3)	2.376(3), 2.358(3)	2.368(2)
Ag-N(4)	2.136(3)	2.137(3), 2.127(3)	2.212(2)
	bond angles		
N(1)-Ag-N(3)	71.4(1)	70.5(1), 71.1(1)	70.9(1)
N(1)-Ag-N(4)	154.7(1)	150.8(1), 150.5(1)	147.6(1)
N(3)-Ag-N(4)	133.9(1)	138.7(1), 138.4(1)	140.6(1)

Due to the presence of the N-H group on the imidazole ring, the crystal packing of derivative **10'** is characterized by the formation of chains of molecules joint together through N-H—O hydrogen bond interactions [N(5)---O(3)^{i} 2.758(3) Å, N(5)-H(5a)—O(3) 167.2°, *i* = x-1, y-1, z; N(10)---O(1)^{ii} 2.800(4) Å, N(10)-H(10a)—O(1) 169.0°, *ii* = x-1, y-1, z-1]. Chains of co-planar molecules are linked between each other with C-H—F interactions, forming layers mostly in the *ab* plane [C(6)---F(4) ^{iii} 3.438(6) Å, C(6)-H(6a)---F(4) 160.9°, *iii* = 2-x, 2-y, -z] (Figure 8a).

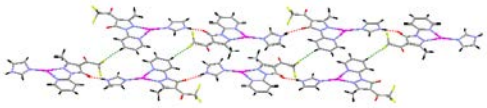

(a)

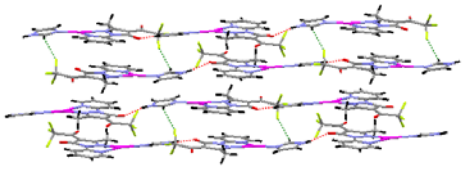

(b)

Figure 8. Crystal packing views of **[Ag($Q^{py,CF3}$)(imH)] (10**$^{'}$**)** showing the network of intermolecular interactions within layers (a) and between layers (b).

As shown in Figure 8b, the repetition of layers along the c axis, gives rise to columns of molecules packed in opposite direction and alternatively interacting through fluorine atoms with upper and/or above hydrogen atoms of imidazole rings [C(12)---F(3) ^{iv} 3.239(5) Å, C(6)-H(6a)---F(4) 131.8°, *iv* = 2-x, 1-y, -z].

On the other hand, in absence of the N-H group on the imidazole ring in derivative *12*, association of complementary molecules into dimers is reached through weak C-H—O=C hydrogen bonds [C(6)---O(1) ^{i} 3.212(4) Å, C(6)-H(6a)—O(1) 139.7°, *i* = -x, -y, 1-z], with the formation of a hydrogen bond ring $R_2^2(14)$ graph set (Figure 9).

Figure 9. Crystal packing views of **[Ag($Q^{py,CF3}$)(Me3py)] (12)** showing the association of complementary molecules in dimers.

Preparation and Characterization of Polyethylene Composite Plastics

Novel PE composite materials were prepared by embedding the Ag(I) derivatives **1-12** in a polyethylene matrix in a 1:1000 weight ratio. The embedding procedure is reported in the Experimental Section, and it is essentially based on heating the mixture containing the Ag(I) derivatives in powdered form and PE granular powder up to the melting point of PE, while stirring to give a homogeneous dispersion, and then cooling to r.t. After solidification, the loaded PE was cut in the form of small disks of 6 mm diameter and of thickness in the range 0.8 - 1.0 mm. The PE composites were characterized by IR and TGA analyses. Composites didn't display any detectable change of their infrared (Figure S1) and thermal properties (Figure S2) with respect to unloaded PE, apart decomposition with progressive weight loss of PE that begins about twenty degrees before PEcomposites.The surface characterization of PE composites was carried out by EDX and SEM analyses. As an example,

Commentato [N1]: da rinumerare

Commentato [N2]: da rinumerare

the SEM spectrum of PE composite containing derivative **1** is shown in Figure 10.

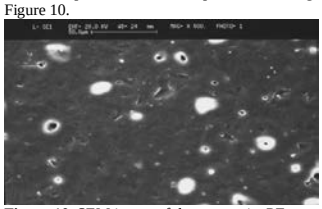

Figure 10. SEM image of the composite PE material containing derivative **1**.

The EDX analysis performed confirmed the presence of silver on the composites material (see EDX spectrum in Figure S3). In the SEM image, black area is PE matrix and white parts are the Ag(I) derivative **1**. The SEM micrograph demonstrates that Ag(I) additive is well dispersed in the polymeric matrix with a wide size distribution (between 20 and 10 nm, although many are less than 10 nm).

Killing Kinetic Tests on PEn Composite Disks

The antibacterial activity of polyethylene composites **PEn** (**n** = **1-12**), containing Ag(I) derivatives **1-12**respectively,was studied after their incorporation into a polyethylene matrix. Two Gram-negative bacteria, *E. coli* and *P. aeruginosa*, and one Gram-positive, *S. aureus*, were selected as models. Unloaded and loaded PE disks with $AgNO_3$ (indicated as **PE0** and**PEAgNO$_3$**, respectively) were tested as negative and positive controls, respectively. Prior to the microbiological studies, the PE disks were prepared and the bacterial cultures were grown as described in the Experimental Section. The killing kinetic tests carried out with PE disks **PE1-PE12** showed different performances, in terms of time and rate of action (Figures 11-13; data shown in terms of CFU and percentage reduction).

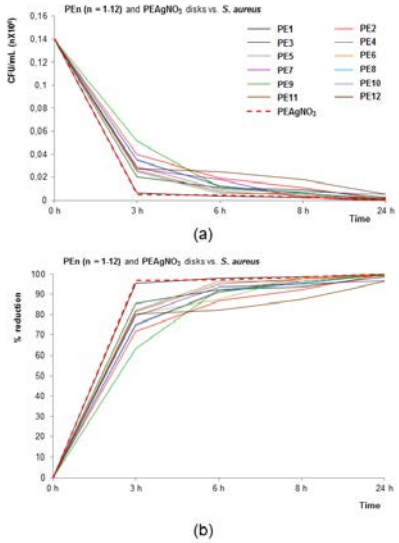

Figure 11. Kinetic killingof **PEn** disks as a function of time, expressed in terms of CFU (a) and percentage reduction (b), against *S. aureus*.

Except **PE12,** all **PEn** disks reached and passed a 90% percent reduction of *S. aureus* within 8 h of exposure, yet with a different rate than in the case of **PEAgNO$_3$** (Figures 11a and b). Only **PE1** showed the same trend of **PEAgNO$_3$** reaching a 97.7% percent reduction in 6 h only. The other **PEn** disks showed a slower activity but almost all reached a 96% percent reduction within 24 h of exposure, except **PE3**, **PE7**, **PE10** and **PE12**.

The latter disks exhibited slower performances, even if they reached 96% of reduction within 24 h. A similar behavior was appreciated for all tested **PEn** disks against *P. aeruginosa* (Figures 12a and b). Except **PE1**, **PE6** and **PE9**, all disks passed a 90% of reduction within 6 h of exposure. In moredetails**, PE10** and **PE12** are comparable to **PEAgNO$_3$**and strongly effective in the first period of exposure, with a 90% of reduction obtained in just 3 h.

Commentato [N3]: da rinumerare

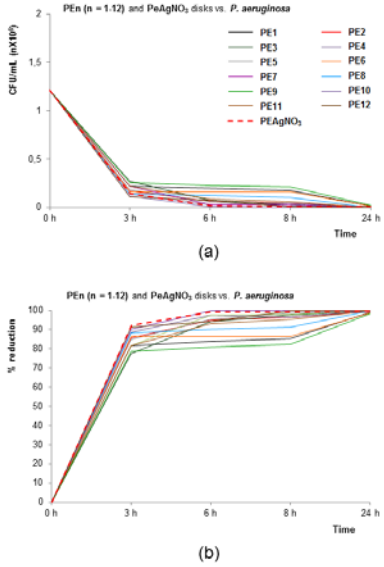

Figure 12. Kinetic killingof **PEn** disks as a function of time, expressed in terms of CFU (a) and percentage reduction (b), against *P. aeruginosa*.

Notably, a markedly different behavior was observed between **PEn**disks against *E. coli* and also between **PEn** and **PEAgNO$_3$** (Figure 13a and b).In fact, all **PEn** showed a slower activity than that displayed against *P. aeruginosa* and *S. aureus*:about 90% reduction is obtained within 6 h only by **PE10** and **PE11**. However, almost all **PEn** passed 90% of reduction within 24 h of exposure.

The different behavior of loaded PE disks **PEn** against the three bacteria strains could be explained by the structure of cell wall in different bacteria strains. To be effective, a biocide needs to bind to the bacterial cell wall. However, the cell wall structure is different in Gram-negative and Gram-positive bacteria. The Gram-negative bacteria (like *E. coli*) have an outer membrane barrier outside of the cell wall.[33] This membrane is formed by lipopolysaccharides (LPS) and proteins, which represent an additional barrier for foreign macromolecules.[34] Gram-positive bacteria (like *S. aureus*)

have a cell wall characterized by a less complex structure.[35] Therefore, the lower performance resulted against *E. coli* than *S. aureus* and the difference activity could be clarified by the cell structure of bacteria. As observed above, the different cellular structure also could explain the lower activity against *E. coli* than *P.aeruginosa* (both Gram-negative bacteria). To disorganize the outer membrane of Gram-negative bacteria the loaded **PEn** disks probably bind to negatively charged LPS membrane, affecting the membrane potential with a consequent disorganization of the outer membrane and cellular death.[36]

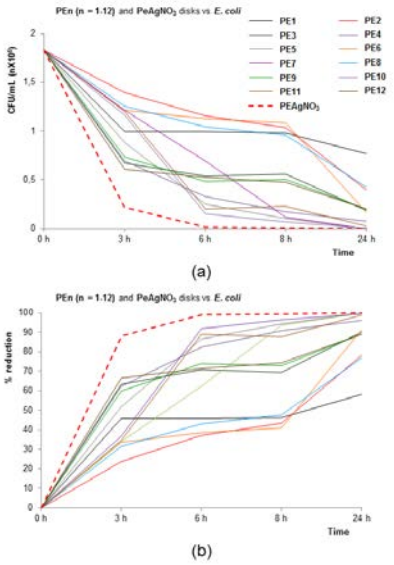

Figure 13. Kinetic killingof **PEn** disks as a function of time, expressed in terms of CFU (a) and percentage reduction (b), against *E. coli*.

Studies about the negatively charged density on cell surface showed that different Gram-negative bacteria possess different negative charges.The diverse results in activity of **PEn** disks against different Gram-negative bacteria (**PEn** are less active against *E. coli* than against *P. aeruginosa*) could be explained by the higher negative charged density on cell surface of *P. aeruginosa* with respect to that in *E. coli*.[37]This should increase the binding strength between silver centers and the component of the cell membrane carrying negative charge density, so that impairing cell respiration by blocking its energy system and resulting in cell death.[38] In summary, the simple polymeric AgQ derivatives **1** and **6** seem to be among the most active additives as an average.

The **test by contact** of the loaded PE disks was carried out on **PE1**, **PE3** and **PE6** composites, in order to have different structural types (polymeric and ionic) of additives used. **PEAgNO$_3$** and **PE0** were used in the test as positive and negative controls. Apart the simple PE disk (**PE0**) all the other composite materials demonstrated inhibition of *E. coli* growth on the contact surface (Figure 14).

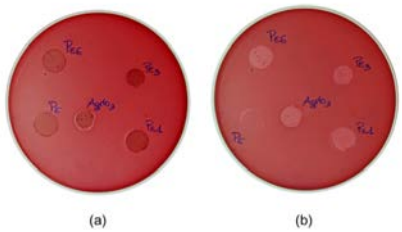

Figure 14. Bactericidal effect promoted by contact with disks of composite **PE1**, **PE3**, **PE6** and **PEAgNO$_3$** (indicated in the photos as AgNO$_3$)compared to the effect of a non-embedded PE disk (indicated in the photoes as PE) for *Escherichia coli* ATCC 25922 with MacConkey agar: (a) bacterial growth can be appreciated only below the non-embedded PE disk; the **PEAgNO$_3$** showsa zone of inhibition around the disk. (b) the picture was taken after lifting the disks:the growth below the PE disk is clearly visible, whereas below the **PE1**, **PE3**, **PE6** and **PEAgNO$_3$**disks there is absence of bacterial growth.

Release tests for specific migration of silver from PEn composite squares.

Release tests from PE composites were carried out for composites **PE1**, **PE3**, **PE4**, **PE6**, and **PE7**,in order to further confirm the mechanism of antimicrobial action by contact. The migration has been tested using three simulants (distilled water, acetic acid 3% v/v and ethanol 10% v/v) at two assay conditions (40°C for 10 days and 80°C for 2 hours), according to EU Legislation on chemicals' migration from plastic materials.[39] The test conditions corresponds to the more severe (worst foreseeable) conditions of contact. **PE0** and **PEAgNO$_3$** squares (Figure S4) were tested as negative and positive controls, respectively.

Commentato [N4]: da rinumerare

A significantly different release was observed between **PEn**squares (**n** = **1**, **3**, **4**, **6** and **7**) and **PEAgNO$_3$** in both conditions of contact (tables 4 and 5).
In fact, all **PEn** showed less release than that of **PEAgNO$_3$**. Such difference could be explained by the insolubility of derivatives **1**, **3**, **4**, **6** and **7** in water with respect to water soluble silver nitrate, which facilitates the migration of silver ions in simulants. Furthermore, **PE1** and **PE6** contain polymeric silver(I) derivatives, and likely for this reason they showed the lesser release among all tested samples.

Table 4 Specific Ag^+migration from **PEn** square composites with embedded silver(I) derivatives **1, 3, 4, 6** and **7,** expressed in terms of percentage release in several simulants by heating at 80°C for 2 hours.

Sample	Simulant A Distilled water	Simulant B Acetic acid 3% v/v	Simulant C Ethanol 10% v/v
Distilled water	0.00		
Acetic acid 3% v/v		0.00	
Ethanol 10% v/v			0.00
PE0	0.00	0.00	0.00
PEAgNO3	100.00	100.00	76.00
PE1	0.51	1.19	0.68
PE3	14.51	9.52	4.08
PE4	5.71	18.57	4.05
PE6	1.84	2.51	1.51
PE7	0.48	6.19	2.86

On the contrary, no significant difference was observed in **PE4** and **PE7** composites, both loaded with monomeric silver(I) derivatives **4** and **7**. **PE3**, loaded with the ionic silver(I) derivative **3**, showed a slightly higher release then the other two composites.
Of course, tests in acetic acid as acidic simulant give the highest values of migration but, even in this case, **PE1** and **PE6** performances are very good, in terms of limited silver release.

Table 5 Specific Ag^+migration from **PEn** square composites with embedded silver(I) derivatives **1, 3, 4, 6** and **7,** expressed in terms of percentage release in several simulants by heating at 40°C for 10 days.

Sample	Simulant A	Simulant B	Simulant C
	Distilled water	Acetic acid 3% v/v	Ethanol 10% v/v
Distilled water	0.00		
Acetic acid 3% v/v		0.00	
Ethanol 10% v/v			0.00
PE0	0.00	0.00	0.00
PEAgNO3	100.00	100.00	55.00
PE1	0.68	2.33	0.60
PE3	5.90	7.09	2.87
PE4	8.10	12.40	8.4
PE6	0.67	4.16	1.27
PE7	2.14	19.27	2.56

CONCLUSIONS

The reaction between twomultitopicacylpyrazolonate ligands and $AgNO_3$ in the presence of base yielded two new coordination polymers (derivatives **1** and **6**). By using also N-donor ancillary ligands it is possible to control the nuclearity, and neutral mono- or dinuclear species have been isolated (**2**, **4**, **5** and **7-12**), apart in one case where an ionic compound afforded (derivative **3**). All derivatives **1-12** have been embedded in polyethylene to give **PEn** composite materials with a 1:1000 weight ratio of additive : PE. Their relevant spectral and thermal properties are essentially unchanged with respect to simple PE, even if the surface of composite PE disks displays a homogeneous dispersion of the additive, which appears as small granules with an average diameter in the range 10-20 μm.
The PE composite materials display an excellent antimicrobial activity against three bacterial strains (the Gram-positive *S. aureus* and Gram-negative *E.coli* and *P. aeruginosa*). The silver coordination polymers (derivatives **1** and **6**) seem the most suited to be used as cheap antimicrobial additives to PE. As an average, they are in fact the most active additives, moreover, they are clearly easier to prepare and less expensive than all the others. Their synthesis does not require any additional reactant, while the other derivatives need also the use of ancillary N-donor ligands, and their isolation is straightforward, by simple filtration from the reaction mixture.
Tests by contact and release tests confirm that, at least for the composite materials containing the two silver(I) coordination polymers (derivatives **1** and **6**), the antimicrobial activity is performed by simple contact of the active surface, without any release of the biocide. The samples of **PEn** composite materials can be re-used several times, displaying always the same antimicrobial activity.
This feature can be appropriate for the application of composite plastics with the above mentioned additives in a number of different situations, such as cases for mobile phones, power buttons in kitchens and remote controls and light switches in hotels, where accumulation of dirt is often overlooked and bacteria levels reach those of the toilet and the bathroom sink.[40]

EXPERIMENTAL SECTION

Materials and Methods.

All chemicals were purchased from Aldrich (Milwaukee) and used as received. The acylpyrazolone ligands HQ^{Ph} (3-methyl-1-phenyl-4-benzoyl-5-pyrazolone) and $HQ^{py,CF3}$ (1-(2-pyridyl)-3-methyl-4-trifluoro acetyl-5-pyrazolone) were synthesized as previously reported.[20,21c] All of the reactions and manipulations were performed in the air. Solvent evaporations were always carried out under vacuum conditions using a rotary evaporator. The samples for microanalyses were dried *in vacuo* to constant weight (20 °C, ca. 0.1 Torr). Elemental analyses (C, H, N) were performed in-house with a Fisons Instruments 1108 CHNS-O Elemental Analyzer. IR spectra were recorded from 4000 to 400 cm^{-1} with a Perkin-Elmer Spectrum 100 FT-IR instrument by total reflectance on a CdSe crystal. ^1H, $^{13}C\{^1H\}$, and $^{19}F\{^1H\}$ NMR spectra were recorded on a 400 Mercury Plus Varian instrument operating at room temperature (400 MHz for ^1H, 100 MHz for ^{13}C, and 376.8 MHz for ^{19}F). H and C chemical shifts (δ) are reported in parts per million (ppm) from $SiMe_4$ (^1H and ^{13}C calibration by internal deuterium solvent lock) while F chemical shifts (δ) are reported in ppm versus $CFCl_3$. Peak multiplicities are abbreviated: singlet, s; doublet, d; triplet, t; quartet, q; and multiplet, m. Melting points are uncorrected and were taken on an STMP3 Stuart scientific instrument and on a capillary apparatus. The electrical conductivity measurements (Λ_M, reported as S cm^2 mol^{-1}) of acetonitrile, methanol and DMSO solutions of the silver derivatives were taken with a Crison CDTM 522 conductimeter at room temperature (r.t.). The positive and negative electrospray mass spectra were obtained with a Series 1100 MSI detector HP spectrometer, using an acetonitrile mobile phase. Solutions (3 mg/mL) for electrospray ionization mass spectrometry (ESI-MS) were prepared using reagent-grade acetonitrile and methanol. For the ESI-MS data, mass and intensities were compared to those calculated using IsoPro Isotopic Abundance Simulator, version 3.1. Peaks containing silver(I) ions were identified as the center of an isotopic cluster. Thermal gravimetric analyses (TGA) were carried out in a N_2 stream with a Perkin-Elmer STA 6000 simultaneous thermal analyzer (heating rate: 7°C/min). Energy dispersive X-ray analyses were carried out in a N2 stream with 800 HS Shimadzu and SEM spectra with a Cambridge Stereoscan 360 Scanning electron Microscope. ICP analyses for specific silver ions migration were carried out with a 7500 cx Agilent Technologies ICP-MS Spectrometer.

Synthesis of [Ag(Q^{Ph})] (1). A methanol solution (30mL) of the ligand HQ^{Ph} (0.278 g, 1.0 mmol) and NaOMe (0.054 g, 1.0 mmol) was added to a water solution (10mL) of silver nitrate (0.170 g, 1.0 mmol). A colorless precipitate immediately resulted, which was filtered off, washed with Et_2O (20 mL), dried in vacuo to constant weight, and shown to be compound **1**. Yield 86% . It is soluble in DMSO. Mp: 234-236°C. Anal. Calcd for $C_{17}H_{13}AgN_2O_2$: C, 53.01; H, 3.40; N, 7.27%. Found: C, 52.69; H, 3.29; N, 7.21%. Λ_M in DMSO: 15.2 S cm^2 mol^{-1}. IR (cm^{-1}) data: 3055w ν(C_{arom}-H), 1612vs, 1592s ν(C=O), 1575m, 1499vs, 1428s, 1354 ν(C=C, C=N, C-N), 1222w, 1064w, 941s, 753s. ^1H NMR (DMSO-d_6): δ 2.18s (3H, C3-CH_3), 7.07t, 7.27-7.33m, 7.36d, 7.60d, 7.77d (10H, H_{arom} of Q^{Ph}). $^{13}C\{^1H\}$ NMR (DMSO-d_6): δ 17.8s (C3-CH_3), 102.0s (*C*4), 120.8s, 123.9s, 127.0s, 128.4s, 128.5s, 129.6s, 139.8s, 141.5s (C_{arom} of Q^{Ph}), 152.6s (*C*3), 163.4s (*C*5), 188.4s (*CO*). TGA-DTA (mg% vs. °C): heating from 30 to 600°C with a speed of 8°C/min; from 230 to 600°C progressive decomposition, with a final black residual of 45% weight.

Synthesis of [Ag(Q^{Ph})(imH)] (2). Imidazole (0.035 g, 0.514 mmol) was added to an acetonitrile suspension (30 mL) of [Ag(Q^{Ph})] (**1**) (0.100 g, 0.26 mmol). A colorless precipitate slowly formed. After 1 h, the solvent was removed almost on rotary evaporator and the precipitate afforded, which was filtered off, washed with methanol (10 mL). After filtration, the colorless powder was dried in vacuo to constant weight and shown to be derivate **2**. Yield 68%. It is soluble in DMSO. Λ_M in DMSO: 24.6 S cm^2 mol^{-1}. Mp: 179-181°C. Anal. Calcd for $C_{20}H_{17}AgN_4O_2$: C, 53.00; H, 3.78; N, 12.36%. Found: C, 52.62; H, 3.73; N, 12.74%. IR (cm^{-1}) data: 3029w, 2727w ν(C_{arom}-H), 1653s, 1580m ν(C=O), 1531s, 1465vs, 1329m ν(C=C, C=N, C-N), 1078s, 913s, 824m. ^{1}H NMR (DMSO-d_6): δ 2.3s (C3-CH_3), 7.60d-8.00s (3H, *H*2, *H*4and *H*5of imH), 6.91t, 7.63t, 8.03, 8.81 (10H, H_{arom} of Q^{Ph}). ^{13}C{^{1}H} NMR (DMSO-d_6): δ 18.3s (C3-CH_3), 102.5s (*C*4), 127.6s, 129.0s, 129.3s, 130.0s, 141.1s, 142.4s (C_{arom} of Q^{Ph}), 120.4s, 123.7s, 138.4s (C_{arom} of imH), 152.8s (*C*3), 164.5s (*C*5), 188.5s (*CO*). TGA-DTA (mg% vs. °C): heating from 30 to 600°C with a speed of 8°C/min; from 198 to 600°C progressive decomposition, with a final black residual of 34% weight.

Synthesis of [Ag(imH)$_2$](Q^{Ph}) (3). Imidazole (0.068 g, 1.0 mmol) was added to an acetonitrile suspension (30 mL) of [Ag(Q^{Ph})] (**1**) (0.100 g, 0.26 mmol). The yellow solution was stirred at room temperature for 24h, the solvent was reduced to two third of the original volume and by slowly evaporation yellow-orange good-quality crystals formed. Yield: 82%. It is soluble in acetonitrile and DMSO. Mp: 154-155°C. Anal. Calcd for $C_{23}H_{21}AgN_6O_2$: C, 52.99; H, 4.06; N, 16.12%. Found: C, 53.05; H, 4.06; N, 16.84%. Λ_M in DMSO: 17.2 S cm^2 mol^{-1}. IR data: 3124m, 2937m ν(C_{arom}-H), 1619s, 1582m ν(C=O), 1520s, 1490m, 1460s ν(C=C, C=N, C-N), 1327s, 1264w, 1146w, 1077s, 827s. ^{1}H NMR (CD_3CN): 2.18s (C3-CH_3 of Q^{Ph}), 7.04s, 7.31s, 8.02s (6H, H_{arom} of imH), 7.04d, 7.29-7.34m, 7.61dd, 7.65dd (10H, H_{arom} of Q^{Ph}). ESI-MS (+, CH_3CN) m/z (%): 226 (87) [(imH)Ag(MeOH)(H_2O)]$^+$, 338 (100) [(HQ^{Ph})(CH_3CN)(H_3O)]$^+$, 444 (8) [Ag(Q^{Ph})(CH_3CN)(H_2O)]$^+$, 611 (22) [Ag_2(Q^{Ph})(imH)(MeOH)(H_2O)]$^+$. TGA-DTA (mg% vs. °C): heating from 30 to 600°C with a speed of 8°C/min; from 150 to 600°C progressive decomposition, with a final black residual of 33% weight.

Synthesis of [Ag(Q^{Ph})(Meim)$_2$] (4). 1-Methylimidazole (0.043 g, 0.52 mmol) was added to an acetonitrile suspension (30 mL) of [Ag(Q^{Ph})] (**1**) (0.100 g, 0.26 mmol). The yellow solution was stirred at room temperature for 24h, the solvent was reduced to one third of the original volume and by slowly evaporation yield yellow-orange good-quality crystals. Yield: 73%. It is soluble in acetonitrile, chloroform and DMSO. Mp: 135-136°C. Anal. Calcd for $C_{25}H_{25}AgN_6O_2$: C, 54.66; H, 4.59; N, 15.30%. Found: C, 54.78; H, 4.51; N, 14.90%. Λ_M in acetonitrile: 50.4 S cm^2 mol^{-1}. IR (cm^{-1}) data: 3104w ν(C_{arom}-H), 1621s, 1587s ν(C=O), 1548m, 1509m, 1418s ν(C=C, C=N, C-N), 1355w, 1246s, 1213m, 1107s, 907s, 710vs. ^{1}H NMR ($CDCl_3$): δ 2.10s (C3-CH_3 of Q^{Ph}), 3.65s (N-CH_3 of 1-MeImH), 6.88s, 6.96s, 7.44s (6H, H_{arom} of Meim), 7.12t, 7.30-7.36m, 7.67dd, 7.83dd (10H, H_{arom} of Q^{Ph}). ^{13}C{^{1}H} NMR ($CDCl_3$): δ 17.8s (C3-CH_3), 34.0s (N-CH_3 of Meim), 120.5s, 124.8s, 139.0s (C_{arom}ofMeim), 103.8s (*C*4), 121.7s, 127.8s, 128.8s, 128.9s, 129.7s, 130.2s, 139.9s, 141.9s (C_{arom} of Q^{Ph}), 152.6s (*C*3), 164.6s (*C*5), 191.0s (*CO*). ESI-MS (+, CH_3CN) m/z (%): 83 (7) [MeimH]$^+$, 271 (100) [Ag(Meim)$_2$]$^+$, 657 (9) [Ag_2(Q^{Ph})(Meim)$_2$]$^+$. TGA-DTA (mg% vs. °C): heating from 30 to 600°C with a speed of 8°C/min; from 100 to 600°C progressive decomposition, with a final black residual of 30% weight.

Synthesis of [Ag(Q^{Ph})(Bzim)] (5). 1-Benzylimidazole (0.094 g, 0.60 mmol) was added to an acetonitrile suspension (15 mL) of [Ag(Q^{Ph})] (**1**) (0.100 g, 0.26 mmol). The yellow solution was stirred at room temperature for 2h, the solvent removed on a rotary evaporator and the brown oil product dissolved in acetone (5 mL) and then Et_2O added (30 mL). A colorless precipitate afforded, which was filtered off, washed with Et_2O (20 mL), dried under reduced pressure (20°C, 0.1 Torr) to constant weight, and shown to be compound **5**. Yield: 40%. It is soluble in chloroform and DMSO. Mp: 68-70°C. Anal. Calcd for $C_{27}H_{23}AgN_4O_2$: C, 59.68; H, 4.27; N, 10.31%. Found: C, 60.62; H, 4.11; N, 10.50%. Λ_M in acetonitrile: 32.4 S cm^2 mol^{-1}. IR (cm^{-1}) data: 3058w ν(C_{arom}-H), 1625s, 1593s ν(C=O), 1497s, 1454s, 1425s ν(C=C, C=N, C-N), 1386m, 1351m, 1218w, 1010w, 943m, 762m, 748vs, 657s. ^{1}H NMR ($CDCl_3$): δ 2.10s (C3-CH_3 of Q^{Ph}), 5.12s (CH_2-N of Bzim), 7.15s, 7.17d, 7.27t, 7.37t, 7.42-7.46m, 7.63d, 7.88d (10H, H_{arom} of Q^{Ph} and 8H, H_{arom} of Bzim). ^{13}C{^{1}H} NMR ($CDCl_3$): δ 18.2s (C3-CH_3 of Q^{Ph}), 51.8s (CH_2-N of Bzim), 120.0s, 122.9s, 126.1s, 127.9s, 128.1s, 128.3s, 129.3s, 129.5s, 130.4s, 138.7s, 141.9s (C_{arom} of $Q^{Ph}$and Bzim). ESI-MS (+, CH_3CN) m/z (%): 159 (92) [BzimH]$^+$, 218 (7) [(Bzim)(CH_3CN)(H_3O)]$^+$, 338 (100) [(HQ^{Ph})(CH_3CN)(H_3O)]$^+$, 946 (9) [Ag_2(Q^{Ph})$_2$(Bzim)(H_2O)]$^+$. TGA-DTA (mg% vs. °C): heating from 30 to 600°C with a speed of 8°C/min; from 150 to 600°C progressive decomposition, with a final black residual of 33% weight.

Synthesis of [Ag($Q^{py,CF3}$)] (6). Derivative **6** was prepared by the same method as **1**.Yield 98%. It is soluble in DMSO, acetone and acetonitrile. Mp: 296-298°C. Anal. Calcd for $C_{11}H_7AgF_3N_3O_2$: C, 34.95; H, 1.87; N, 11.11%. Found: C, 34.95; H, 1.65; N, 10.68%. Λ_M in acetonitrile: 20.6 S cm^2 mol^{-1}. IR (cm^{-1}) data: 1649vs, 1593m ν(C=O), 1501s, 1432s ν(C=C, C=N, C-N), 1345s, 1248m, 1180s, 1119s, 1069m, 952s, 779s. ^{1}H NMR (CD_3CN): δ 2.40s (3H, C3-CH_3), 7.12dd, 7.86d, 8.26dd, 8.79d (4H, N1-C_5H_4N). ^{13}C{^{1}H} NMR (CD_3CN): δ 19.3s (C3-CH_3), 99.4s (*C*4), 118.9q (*C*F_3), 114.5s, 120.5s, 140.8s, 149.4s, 156.2s (C_{arom} of $Q^{py,CF3}$), 151.8s (*C*3), 164.5s (*C*5), *C*O not observed. ^{19}F{^{1}H} NMR (CD_3CN): δ -75.98s (*C*F_3) (T = 293 K). ESI-MS (+, CH_3CN) m/z (%): 222 (100) [Ag(CH_3CN)$_2$(CH_3OH)]$^+$, 600 (35) [Ag_2($Q^{py,CF3}$)(CH_3CN)$_2$(CH_3OH)]$^+$. TGA-DTA (mg% vs. °C): heating from 30 to 600°C with a speed of 8°C/min; from 260 to 600°C progressive decomposition, with a final black residual of 40% weight.

Synthesis of [Ag($Q^{py,CF3}$)(Bzim)] (7).Derivative **7** was obtained similarly to **2**. Mp: 136-138°C. Anal. Calcd for $C_{21}H_{17}AgN_5O_2F_3$: C, 47.03; H, 3.20; N, 13.06%. Found: C, 46.29; H, 2.80; N, 12.68%. IR (cm^{-1}) data: 3112w ν(C_{arom}-H), 1661s, 1610vs ν(C=O), 1537m, 1471m, 1435s, 1331m, 1259m ν(C=C, C=N, C-N), 1183s, 1144vs, 1007m, 922m, 774vs.

Synthesis of [Ag($Q^{py,CF3}$)(2Mebzim)] (8). Derivate **8** was obtained similarly to**7**. Mp: 225-226°C. Anal. Calcd for $C_{22}H_{19}AgN_5O_2F_3$: C, 48.02; H, 3.48; N, 12.73%. Found: C, 47.69; H, 3.10; N, 12.44%. IR (cm^{-1}) data: 1660s, 1631vs, ν(C=O), 1595m, 1487w, 1465s, 1434s, 1329 ν(C=C, C=N, C-N), 1189s, 1137vs, 1007m, 923m, 775vs.

Synthesis of [Ag($Q^{py,CF3}$)(2EtimH)] (9). Derivative **9** was obtained similarly to**8**. Mp: 256-258°C. Anal. Calcd for $C_{16}H_{15}AgN_5O_2F_3$: C, 40.53; H, 3.19; N, 14.77%. Found: C, 40.22; H, 2.80; N, 14.03%. IR (cm^{-1}) data: 3101w ν(C_{arom}-H), 1608s ν(C=O), 1529m, 1490m, 1462s, 1432s ν(C=C, C=N, C-N), 1331s, 1258m, 1149s, 919s, 723vs.

Synthesis of [Ag_2($Q^{py,CF3}$)$_2$(COdim)] (10). Derivative **10** was obtained similarly to**8**. Mp: 246-248°C. Anal. Calcd for $C_{29}H_{20}Ag_2F_6N_{10}O_5$: C, 37.93; H, 2.20; N, 15.25%. Found: C, 37.91; H, 2.18; N, 15.53%. IR (cm^{-1}) data: 3160m ν, 3070w ν(C_{arom}-H), 1662m, 1622s ν(C=O), 1529m, 1490m, 1466s, 1434s ν(C=C, C=N, C-N), 1335s, 1304m, 1259s, 918s, 724vs.

Synthesis of [Ag($Q^{py,CF3}$)(2tfbimH)] (11). Derivate **11** was obtained similarly to**8**. Mp: 289-290°C. Anal. Calcd for $C_{19}H_{12}AgN_5O_2F_6$: C, 40.45; H, 2.14; N, 12.41%. Found: C, 41.03; H, 1.81; N, 11.99%. IR (cm^{-1}) data: 3072w ν(C_{arom}-H), 1678m, 1605s, 1596s ν(C=O), 1530m, 1474m, 1438s, 1331m, 1259m ν(C=C, C=N, C-N), 1194s, 1144vs, 1007m, 920m, 776vs.

Synthesis of [Ag($Q^{Py,CF3}$)(Me3py)] (12). Derivate **12** was obtained similarly to**8**. Mp: 245-246°C. Anal. Calcd for $C_{19}H_{18}AgN_4O_2F_3$: C, 45.71; H, 3.63; N, 11.22%. Found: C, 45.17; H, 3.19; N, 10.68%. IR (cm^{-1}) data: 3074w ν(C_{arom}-H), 1661m, 1617s, 1593s ν(C=O), 1528m, 1469m, 1433s, 1331m, 1256m ν(C=C, C=N, C-N), 1177s, 1139vs, 1007m, 916vs, 773vs.

All other analytical and spectroscopic data of derivatives **7-12** are available as Supporting Information.

Solid State NMR Spectroscopy. ^{15}N SS NMR spectra were recorded on a BrukerAvance II 400 instrument operating at 400.23 and 40.55 MHz for ^{1}H and ^{15}N nuclei, respectively. Cylindrical 4 mm o.d. zirconia rotors with a sample volume of 80 μL were employed and spun at 9 kHz. A ramp cross-polarization pulse sequence was used with a contact time of 4 ms, a ^{1}H 90° pulse of 3.05 μs, recycle delays of 10-20 s, and 16000-20000 transients. A two pulse phase modulation (TPPM) decoupling scheme was used with an rf field of 75 kHz. ^{15}N chemical shifts were referenced with the resonance of $(NH_4)_2SO_4$ (^{15}N signal at δ = 355.8 ppm with respect to CH_3NO_2).

Crystal structure analyses. Details of the crystal data collection are listed in Table 6. X-ray data for **3**, **4**, **7, 8** , **10**' and **12** were collected on a Bruker-Nonius X8 Apex CCD area detector equipped with graphite monochromator and Mo Kα radiation (λ = 0.71073 Å), and data reduction was performed using the SAINT programs; absorption corrections based on multiscan were obtained by SADABS.[41] Both structures were solved by Patterson method (SHELXS/L program in the SHELXTL-NT software package) and refined by full-matrix least-squares based on F^2.[42] All non-hydrogen atoms were refined anisotropically, and all hydrogen atoms were included as idealized atoms riding on the respective carbon atoms with C–H bond lengths appropriate to the carbon atom hybridization.

Silver(I) derivativesembedding in polyethylene disks. Polyethylene (PE) disks with embedded the complexes **1-12** were prepared in the following manner: the coordination polymer, in the form of powder, was mixed in a glass capsule with PE granular powder (1.00 g) in a 1:1000 weight ratio. The capsule was heated up to the melting point of PE (98 °C), while its content was stirred to give a homogeneous dispersion. The dispersion was then left to cool at room temperature; after solidification, the loaded polymer matrix was removed from the capsule and placed in contact with a hot quartz surface (130 °C): within a few minutes, the matrix melted and distributed homogeneously onto the quartz surface to give a thin liquid layer. After reduction of the quartz surface temperature down to 80 °C, the polymeric matrix layer turned into a soft solid film, suitable to be cut into small disks of 6 mm diameter and of thickness in the range 0.8 - 1.0 mm.

Microbiological studies. The antibacterial activity of all PE composite disks containing the Ag(I) derivatives was tested against the two Gram-negative bacteria *E. coli* ATCC 25922 (PBI International) and *P. aeruginosa* ATCC 27853 (OXOID-remel) and the Gram-positive bacterium *S. aureus*ATCC 25923 (BPI International). Bacteria were grown aerobically at 37°C for 18 hours using Tryptone Soya Broth (OXOID) as the growth medium. Bacterial cultures (10^6 CFU/mL) were added to sterilized test tubes containing 4 mL of autoclaved physiological solution. For sterilization of the tubes, an Alfa-10-plus autoclave (PBI International) was used, operating at 121 °C for 15 min. A 40 mg amount of loaded **PEn** disk, previously reduced to granules, was added to the test tubes containing bacterial suspensions. All tubes were kept on an IKA KS 130 BASIC agitator for 24 hours at slow speed. To study the growth inhibitory effect of the PE composite disks on the bacterial cultures, 100 μL of supernatant fraction were withdrawn from the tubes at time intervals of 3, 8 and 24 hours. To obtain the bacterial colony count, the supernatant fraction was diluted and included uniformly into Petri dishes containing Plate Count Agar (OXOID). Adopting the same procedure, an unloaded PE disk was used as negative control. In addition, we conducted a preliminary test to evaluate the bactericidal effect of the loaded PE disks by contact. To this aim, 0.5 mL of the bacterial aqueous suspension (*E. coli* 10^6 CFU/ ml) was streaked over a plate containing MacConkey Agar, differential medium for the isolation of coliforms and intestinal pathogens in water, dairy products and biological specimens (OXOID S.p.A), and were spread uniformly. Composite **PEn** disks and the blank disk were gently placed over contaminated MacConkey Agar in Petri dishes. Petri dishes were incubated overnight at 35 ° C for 24 hours. After incubation, growth inhibition was evaluated by visual inspection, observing the dish, inverted, on a light table (Precision Illuminator, model B95, Northern Light).

Table 6.Details of data collection and structure refinements for complexes 3, 4, 9, 10′ and 12.

	3	4	9	10′	12
Empirical formula	$C_{23}H_{21}N_6O_2Ag$	$C_{25}H_{25}N_6O_2Ag$	$C_{16}H_{15}N_5O_2F_3Ag$	$C_{28}H_{22}N_{10}O_4F_6Ag_2$	$C_{19}H_{18}N_4O_2F_3Ag$
M_w [g mol^{-1}]	521.33	549.38	474.20	892.30	499.24
crystal system	Triclinic	Triclinic	Orthorhombic	Triclinic	Triclinic
space group	P-1	P-1	Pbcn	P-1	P-1
a [Å]	9.4327(8)	10.716(3)	22.338(5)	11.509(4)	8.347(5)
b [Å]	11.4901(10)	10.771(3)	7.2724(17)	12.161(4)	11.507(5)
c [Å]	11.5353(10)	11.979(4)	22.502(5)	14.131(5)	12.099(5)
α [°]	76.060(2)	64.287(9)	90	96.05(2)	63.053(5)
β [°]	72.454(3)	74.569(9)	90	102.40(2)	83.861(5)
γ [°]	72.186(3)	74.621(9)	90	117.954(16)	74.706(5)
V [Å^3]	1125.82(17)	1182.8(6)	3655.6(14)	1656.7(10)	999.1(8)
Z	2	2	8	2	2
ρ_{calcd} [g cm^{-3}]	1.538	1.543	1.723	1.789	1.659
μ(MoKα)[mm^{-1}]	0.927	0.887	1.154	1.266	1.058
θrange [°]	1.87-30.77	2.49-27.00	2.57-26.31	2.10-27.00	1.89-26.00
Total reflns	27520	41280	6984	30837	12807
unique reflnsR_{int}	6945, 0.0770	5120, 0.0335	3655, 0.0340	7223, 0.0631	3905, 0.0245
obs. reflns [I > 2σ(I)]	4761	4514	2245	4758	3522
no. parameters	290	310	244	451	362
R_1 (obs. Data)	0.0428	0.0299	0.0379	0.0382	0.0273
wR_2(all data)	0.1181	0.0972	0.1027	0.1031	0.0921
S (all data)	0.967	0.990	0.989	1.034	1.097
max. Peak/hole [e Å^{-3}]	0.739/-0.989	0.662/-0.731	0.370/-0.654	0.693/-0.432	0.672/-0.332

Release Tests for specific migration of silver from compositePEn materials.[39]***PEn composite squares preparation.*** Polyethylene squares(Figure S4) with embedded the complexes **1, 3, 4, 6** e **7**were prepared in the following manner: the coordination polymer, in the form of powder was mixed in a Teflon mould, with an area of 1 dm^2, with PE granular powder (7.00 g) in a 3:1000 weight ratio. The Teflon mould was heated up to the melting point of PE (98 °C), while its content was stirred to give a homogeneous dispersion. The dispersion was then left to cool at room temperature; after solidification, the loaded polymer matrix was removed from the mould and was reduced into pieces suitable for migration testing. ***Migration tests.*** Themigration tests were performed under different contact conditions using distilled water (simulant A), 3% acetic acid (simulant B), 10% ethanol v/v (simulant C). Samples were immersed in 100 mL of simulant in a conical flask with ground glass stopper. In this manner both faces of the sample were in contact with the simulant. All conic flasks, covered with a tin foil, were kept in controlled atmosphere at two assay conditions: 40°C for 10 days and 80°C for 2 hours. After the incubation period, pieces were removed and the simulant was treated to analyze the Ag^+ released in the simulants by Inductive Coupled Plasma spectroscopy with Mass Spectrometry detection(ICP-MS). Adopting the same procedure, an unloaded PE square was used as negative control and a loaded PE square with $AgNO_3$ as positive control. A solution containing In (10 µg/L) was used as internal standard for ICP-MS measurements. Calibration curves for investigated element were obtained by using aqueous (3% nitric acid) standard solutions prepared by appropriate dilution of stock standards (Ag standard solution 10mg/l for ICP-MS).

ASSOCIATED CONTENT

Supporting Information. Complete analytical andspectroscopic data for derivatives **7-12**, figures S1 and S2, crystallographic data for derivatives for **3**, **4**, **9**, **10**′ and **12** in CIF Format. This material is available free of charge via the Internet at http://pubs.acs.org.

AUTHOR INFORMATION

Corresponding Authors

*E-mail: claudio.pettinari@unicam.it (C.P.), fabio.marchetti@unicam.it (F.M.), roberto.gobetto@unito.it (R.B.).

Notes

The authors declare no competing financial interest.

ACKNOWLEDGMENT

This work was financially supported by the University ofCamerino (Fondo di Ateneo per la Ricerca 2011-2012) andNuova Simonelli company.

REFERENCES

(1) (a) Muñoz-Bonilla, A.; Fernández-García, M. *Prog. Polym. Sci.***2012**, *37*, 281-339.(b) Kenawy, E.-R.; Worley, S. D.; Broughton, R. *Biomacromol.***2007**, *8*, 1359-1384. (c) Charnley, M.; Textor, M.; Acikgoz, C. *React. Funct. Polym.* **2011**, *71*, 329–334.

(2) (a) Crespy, D.; Landfester, K. *Polymer***2009**, *50*, 1616–1620. (b) Gautam, A.; Ram, S. *Mater. Chem. Phys.* **2010**, *119*, 266–271.

(3) Percival, S. L.; Bowler, P. G.; Russell, D. J. *Hosp. Infect.***2005**, *60*, 1–7.

(4) Amato, E.; Diaz-Fernandez, Y. A.; Taglietti, A.; Pallavicini, P.; Pasotti, L.; Cucca, L.; Milanese, C.; Grisoli, P.; Dacarro, C.; Fernandez-Hechavarria, J. M.; Necchi, V. *Langmuir***2011**, 27, 9165–9173.

(5) (a) Gunawan, P.; Guan, C.; Song, X.; Zhang, Q.; Leong, S. S. J.; Tang, C.; Chen, Y.; Chan-Park, M. B.; Chang, M. W.; Wang, K.; Xu, R. *ACS Nano***2011**, *5*, 10033–10040; (b) Kar, S.; Subramanian, M.; Ghosh, A. K.; Bindal, R. C.; Prabhakar, S.; Nuwad, J.; Pillai, C. G. S.; Chattopadhyay, S.; Tewari, P. K. *Desal. water treat.* **2011**, *27*, 224–230; (c) da Silva Paula, M. M.; Franco, C. V.; Baldin, M. C.; Rodrigues, L.; Barichello, T.; Savi, G. D.; Bellato, L. F.; Fiori, M. A.; da Silva, L. *Mater. Sci. Eng. C.* **2009**, *29*, 647–650; (d) Brady, M. J.; Lisay, C. M.; Yurkovetskiy, A. V.; Sawan, S. P. *Am. J. Infect. Control* **2003**, *31*, 208–214.

(6) Gordon, O.; Slenters, T. V.; Brunetto, P. S.; Villaruz, A. E.; Sturdevant, D. E.; Otto, M.; Landmann, R.; Fromm, K. M. *Antimicrob. Agents Chemother.* **2010**, *54*, 4208–4218.

(7) Choi, O.; Deng, K. K.; Kim, N.-J.; Ross, L.; Surampalli, R. Y.; Hu, Z. *Water Res.* **2008**, *42*, 3066–3074.

(8) Chernousova, S.; Epple, M. *Angew. Chem. Int. Ed.* **2013**, *52*, 1636–1653.

(9) (a) Rai, M.; Yadav, A.; Gade, A. *Biotechnol. Adv.* **2009**, *27*, 76–83;(b) Chou, K.-S.; Ren, C.-Y. *Mater. Chem. Phys.* **2000**, *64*, 241–246; (c) Wong, K. K. Y.; Liu, X. *MedChemComm***2010**, *1*, 125-131; (d) Liu, J.; Sonshine, D. A.; Shervani, S.; Hurt, R. H. *ACS Nano***2010**, *4*, 6903–6913.

(10) Helttunen, K.; Moridi, N.; Shahgaldian, P.; Nissinen, M. *Org. Biomol. Chem.* **2012**, *10*, 2019-2025.

(11) Bullen, J. J.; Rogers, H. J.; Spalding, P. B.; Ward, C. G. *FEMS Immunol. Med. Microbiol.* **2005**, *43*, 325-330.

(12) Pettinari, C.; Marchetti, F.; Lupidi, G.; Quassinti, L.; Bramucci, M.; Petrelli, D.; Vitali, L. A.; Guedes da Silva, M. F. C.; Martins, L. M. D. R. S.; Smoleński, P.; Pombeiro, A. J. L. *Inorg. Chem.***2011**, *50*, 11173–11183.

(13) Tăbăcaru, A.; Pettinari, C.; Marchetti, F.; Di Nicola, C.; Domasevitch, K. V.; Galli, S.; Masciocchi, N.; Scuri, S.; Grappasonni, I.; Cocchioni, M. *Inorg. Chem.***2012**, *51*, 9775–9788.

(14) Marchetti, F.; Pettinari, C.; Pettinari, R. *Coord. Chem. Rev.* **2005**, *249*, 2909-2945.

(15) (a) Cingolani, A.; Effendy, Marchetti, F.; Pettinari, C.; Pettinari, R.; Skelton, B. W.; White, A. H. *Inorg. Chem.* **2002**, *41*, 1151-1161. (b) Cingolani, A.; Effendy, Marchetti, F.; Pettinari, C.; Pettinari, R.; Skelton, B. W.; White, A. H. *Inorg. Chim. Acta***2002**, *329*, 100-112. (c) Cingolani, A.; Effendy, Marchetti, F.; Pettinari, C.; Pettinari, R.; Skelton, B. W.; White, A. H. *Inorg. Chem.* **2004**, *43*, 4387-4399. (d) Lorenzotti, A.; Marchetti, F.; Pettinari, C.; Pettinari, R.; Skelton, B. W.; White, A. H. *Inorg. Chim. Acta***2005**, *358*, 3190-3200.

(22) (a) Siebel, E; Dieter Fischer, R.; Davies, N.A.; Apperley, D. C.; Harris, R. K. *J. Organomet. Chem.* **2000**, *604*, 34–42; (b) Pettinari, R.; Pettinari, C.; Marchetti, F.; Gobetto, R.; Nervi, C.; Chierotti, M. R.; Chan, E. J.; Skelton, B. W.; White, A. H. *Inorg. Chem.* **2010**, *49*, 11205-11215.

(23) Chierotti, M. R.; Gobetto, R. *Eur. J. Inorg. Chem.***2009**, 2581–2597.

(24) Tobbens, D.M.; Glinneman, J.; Chierotti, M. R.; van de Streek, J.; Sheptyakov, D. *Cryst. Eng. Comm.***2012**, *14*, 3046-3055.

(25) (a) Bowmaker, G. A.; Harris, R. K.; Assadollahzadeh, B.; Apperley, D. C.; Hodgkinson, P.; Amornsakchai, P. *Magn. Reson. Chem.***2004**, *42*, 819–826; (b) Bertolasi, V.; Boaretto, R.; Chierotti, M. R.; Gobetto, R.; Sostero, S. *Dalton Trans.* **2007**, 5179–5189.

(26) (a) Gallego, M. L.; Ovejero, P.; Cano, M.; Heras, J. V.; Campo, J. A.; Pinilla, E.; Torres, M. R. *Eur. J. Inorg. Chem.***2004**, 3089–3098. (b) (c) Cornago, P.; Claramunt, R.M.; Cano, M.; Heras, J.V.; Gallego, M. L. *Arkivoc***2005**, *9*, 21-29; (d) Gallego, M. L.; Cano, M.; Campo, J. A.; Heras, J. V.; Pinilla, E.; Torres, M. R.; Cornago, P.; Claramunt, R. M. *Eur. J. Inorg. Chem.* **2005**, 4370-4381.

(27) Levy, G. C.; Lichter, R.L. "Nitrogen-15 Nuclear Magnetic Resonance Spectroscopy", John Wiley & Sons, Inc., New York, 1979.(dove metteremeltestoilriferimento?)

(28) Lorente, P.; Shenderovich, I. G.; Golubev, N.S.; Denisov, G.S.; Buntkowsky, G.; Limbach, H.-H. *Magn. Reson. Chem.***2001**, *39*, S18–S29. (dove metteremeltestoilriferimento?)

(29) Akama, Y.; Shiro, M.; Ueda, T.; Kajitani, M. *ActaCrystallogr., Sect. C: Cryst. Struct. Commun.* **1995**, *51*, 1310-1314.

(30) Scheele, U. J.; Georgiou, M.; John, M.; Dechert, S.; Meyer F. *Organometallics***2008**, *27*, 5146–5151.

(31) Cingolani, A.; Effendy, Marchetti, F.; Pettinari, C.; Pettinari, R.; Skelton, B. W.; White, A. H. *Inorg. Chim. Acta* **2002**, *329*, 100–112.

(32) Nishio, M.; Umezawa, Y.; Honda, K.; Tsuboyama, S.; Suezawa, H. *Cryst. Eng. Comm.***2009**, *11*, 1757-1788.

(33) Kenawy, E. R.; Worley, S. D.; Broughton, R. *Biomacromol.* **2007**, *8*, 1359-1384.

(34) Chen, C. Z.; Beck-Tan, N. C.; Dhurjati, P.; Dyk, T. K.; La Rossa, R. A.; Cooper, S. L. *Biomacromol.* **2000**, *1*, 473-480.

(35) Kong, H.; Jang, J. *Langmuir***2008**, *24*, 2051-2056.

(36) Kügler, R.; Bouloussa O.; Rondelez, F. *Microbiol.***2005**, *151*, 1341–1348 and references therein.

(37) Chung, Y. C.; Su, Y. P.; Chen, C. C.; Jia, G.; Wang, H. L.; Wu, J. C.; Lin, J. G. *ActaPharmacol. Sin.* **2004**, *25*, 932-936.

(38) a) Nawaz, M.; Han, M. Y.; Kim, T. I.; Manzoor, U.; Amin, M. T. *Sci. Total Environ.* **2012**, *431*, 20–25. b) Thurman, R. B.; Gerba, C. P. *Crit. Rev. Environ. Contr.* **1989**, *18*, 295–315.

(39) EU Food Contact Regulations for Plastics (food packaging and food Regulations 1935/2004, 79/112/EEC and 89/109/EEC) and EU Regulation 10/2011 (The Plastics Regulation), which indicates the rules for measuring overall and specific migration. (http://ec.europa.eu/food/food/chemicalsafety/foodcontact/index_eu.htm).

(40) Kirsch, K. R.; Sirsat, S.; Neal, J.; Kline, S.; Almanza, B.; Stroia; O. "A Microbial Analysis of Environmental Surfaces in Hotel Rooms" presented at 112° General Meeting of American Society for Microbiology, San Francisco, California, June 16-19, 2012.

(41) *SMART, SAINT and SADABS*, Bruker AXS, Inc., Madison, WI, 1997.

(42) *SHELXTL-NT Crystal Structure Analysis Package, Version 5.1*, Bruker AXS Inc., Madison, WI, 1999.

Highligths: Novel silver(I) derivatives containing acylpyrazolonate ligands were embedded on polyethylene matrix. The antimicrobial activity of the composite materials was tested against *E. coli*, *P. Aeruginosa* and *S. aureus*. These novel plastic composites show efficient inhibition of bacteria growth on the contact surface, all polymers exceeding 90% percent reduction of bacteria within few hours of exposure. Composites containing silver(I) coordination polymers as additives exert their antimicrobial action by simple contact, without silver ions release.